Early Evaluation of Ku- and Ka-Band Sensitivities for the Global Precipitation Measurement (GPM) Dual-Frequency Precipitation Radar (DPR)

Koichi Toyoshima[1], Hirohiko Masunaga[2] and Fumie A. Furuzawa[2]
[1]*Graduate School of Environmental Studies*, *Nagoya University*, *Nagoya*, *Japan*
[2]*Hydrospheric Atmospheric Research Center*, *Nagoya University*, *Nagoya*, *Japan*

Abstract

The purpose of this paper is to quantify the sensitivity of the Global Precipitation Measurement (GPM) mission core observatory Dual-frequency Precipitation Radar (DPR) with focus on the Ka-band detectability of light rain and snow in comparison with the Ku-band capability. In this work, storm top height (STH) is utilized exclusively as the metric of radar sensitivity. The GPM DPR standard product level 2 version 3 is used in this analysis for the period from April to August 2014. The Ka high sensitivity (HS) mode and Ku have little systematic difference in STH over a broad range of the histogram, implying that the advantage of the Ka HS mode may not be as distinct as expected. The non-Rayleigh scattering effect may have partly offset the sensitivity advantage of the Ka HS over the Ku.

(**Citation**: Toyoshima, K., H. Masunaga, and F. A. Furuzawa, 2015: Early evaluation of Ku- and Ka-band sensitivities for the Global Precipitation Measurement (GPM) Dual-frequency Precipitation Radar (DPR). *SOLA*, **11**, 14−17, doi:10.2151/sola.2015-004.)

1. Introduction

The Global Precipitation Measurement (GPM) mission core observatory was launched in February 2014, carrying the Dual-frequency Precipitation Radar (DPR) developed by the Japan Aerospace Exploration Agency (JAXA) with the National Institute of Information and Communication Technology (NICT). The DPR consists of two radars with the microwave frequencies of Ka band (35.55 GHz) and Ku band (13.6 GHz). A Ku-band radar has been demonstrated by the Tropical Rainfall Measuring Mission (TRMM) Precipitation Radar (PR) to be suitable for measuring moderate to heavy rains typical of the tropical and mid-latitude regions, while a Ka-band radar is expected to extend its ability to capture weak rain and snow in higher latitudes as well (Hou et al. 2008, 2014). Several months of observations from the GPM core observatory are now available, allowing an early evaluation of the instruments onboard. The purpose of this paper is to quantify the sensitivity of DPR with focus on the Ka-band detectability of light rain and snow in comparison with the Ku-band capability. The techniques of rainfall retrieval with a dual-frequency radar have been developed to reduce ambiguity in rain rate retrieval in comparison with single wavelength radars (Chandrasekar et al. 2003; Rose and Chandrasekar 2005; Liao et al. 2005; Liao and Meneghini 2005; Seto et al. 2013; Kubota et al. 2014). In this work, storm top height (STH) is utilized exclusively as the metric of radar sensitivity instead of more conventional measures including surface rain rate. This is because STH is not affected by algorithm assumptions such as drop size distribution and attenuation correction that are indispensable for rainfall retrieval and hence is deemed optimal for studying the instrument performance separately from algorithm uncertainties.

Corresponding author: Koichi Toyoshima, Nagoya University, Furo-cho, Chikusa-ku, Nagoya, Japan. E-mail: toyoshima@satellite.hyarc.nagoya-u.ac.jp

In this paper, the analyzed data are first described in Section 2 and STH is defined in Section 3. The results are presented in Section 4, where the individual Ku- and Ka-radar sensitivity is examined in some detail. Finally, the findings are discussed and concluded in light of potential physical explanations (Section 5).

2. Data

The GPM DPR standard product level 2 version 3 is used in this analysis for the period from April to August 2014. The Ka-band radar has two different scan modes of matched scan (Ka MS) and high sensitivity scan (Ka HS). Ka MS is matched footprint by footprint with the Ku-band radar and has 25 angle bins with the range bin size of 125 m. Ka HS footprints are interlaced with Ku footprints and has 24 angle bins with range bin size of 250 m. The Japanese 55-year Reanalysis (JRA55) (Kobayashi et al. 2015) surface air temperature at 2 m is used to isolate out the condition that precipitation is considered to be entirely freezing.

3. Storm top height

STH in the DPR standard product is defined as the altitude of the highest range bin that contains precipitating echoes, where radar reflectivity is required to exceed a given threshold for 6 successive range bins to filter out noise. Noise analysis for spaceborne radars was given, for example, by Kumagai (1997) and Takahashi and Iguchi (2008). The DPR minimum detectable echo as measured in the pre-launch test is 14.5 dBZ, 16.47 dBZ, and 10.2 dBZ for Ku, Ka MS, and Ka HS, respectively (Kubota, in private communication). These values are better than the nominal sensitivities or 18 dBZ for Ku and 12 dBZ for Ka HS (Hou et al. 2014). These values, however, are not guaranteed to stay valid after the instrument is launched into orbit. In the DPR product, the radar sensitivity estimated with a signal-to-noise ratio threshold is sought for each angle bin based on the noise level determined from echo-free range bins (Kubota, in private communication). This definition of radar sensitivity is robust from an engineering perspective in that it is independent of any arbitrary assumptions except for the additional requirement that 6 continuous bins should all contain echoes above the noise level to define STH. In this paper, STH is recalculated in the same manner as done for the DPR product but by varying the threshold every 2 dBZ from 8 dBZ to 20 dBZ in order to ensure the robustness of STH statistics. The analysis is limited to near-nadir (from 21st to 29th) angle bins in order to minimize the influence of the side robe clutters.

4. Results

The minimum detectable echoes of Ku and Ka radars generally do not precisely agree with the nominal values determined for the success criterion of the GPM mission. The radar sensitivity could be also slightly changed after launch from the measurements at the pre-launch testing. We first evaluate the minimum detectable echoes in orbit with the actual observations and compare them

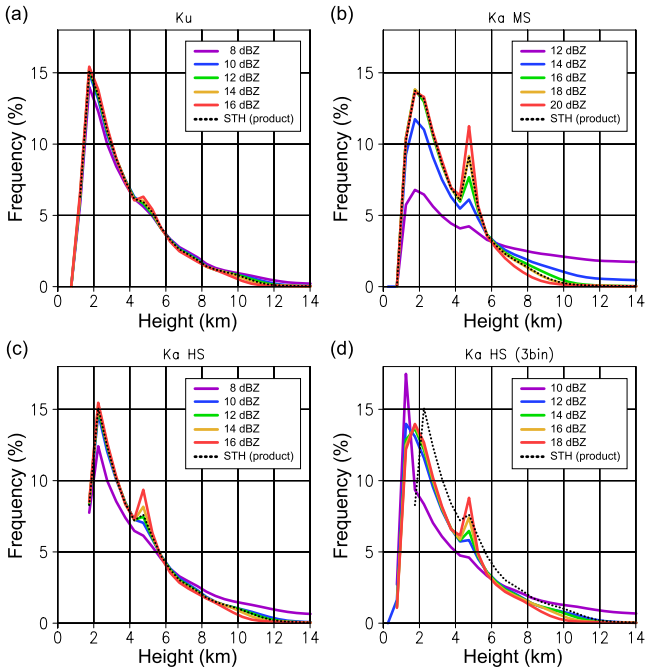

Fig. 1. The normalized histogram of STH for global oceans within the observational coverage of GPM DPR. The reference STH from the GPM standard product is plotted in black, and STHs recalculated with different reflectivity thresholds are delineated in colors as indicated for (a) Ku, (b) Ka MS and (c) Ka HS. (d) The same as (c) but with 3 instead of 6 successive range bins to define STH.

with the nominal and pre-launch values. Figure 1 shows the histogram of STH calculated with several thresholds with the standard product as the reference for global oceans covered by the GPM core satellite. Some noticeable features are evident in the STH histogram. The Ka MS histogram has a sharp spike at 4−5 km that is absent for Ku, which is ascribed to the inability of Ka MS to detect solid precipitation above the melting layer as described later. Note that a similar peak is observed also for Ka HS with artificially high threshold values but is only barely present for a realistic threshold of 12 dBZ. The Ka MS exhibits a striking dependence on the threshold, showing a long tail toward high altitudes for lowest threshold values, which arises once the threshold decreases to far below the noise level. A similar histogram tail is also visible for Ka HS when the reflectivity threshold is decreased to 8 dBZ. These results together suggest a guideline for estimating the minimum detectable echo from the STH histogram. First, the threshold would be too low compared to the actual noise level if a histogram tail arises toward the high end. Second, the threshold might be too high if a fictitious melting-layer spike appears, except for Ka MS where the sensitivity is by design so poor that frozen precipitation is largely missed. A correct threshold should lie between these two extreme cases. Bearing this in mind, the reflectivity threshold in the standard product (black dotted line in Fig. 1) that best reproduces the reference STH roughly is hence estimated to be between 12 and 14 dBZ for Ku (Fig. 1a), 18 dBZ for Ka MS (Fig. 1b) and 12 dBZ for Ka HS (Fig. 1c). These results suggest that estimated minimum detectable echoes in orbit are roughly consistent with the pre-launch values noted above, although the Ku radar sensitivity is slightly better in orbit.

For Ka HS, the STH histogram appears to entirely lack STHs lower than 1.5 km. This is unrealistic because observational evidence shown later (Fig. 2) implies a large population of precipitating clouds with STHs below 1.5 km. The failure to detect shallow precipitation arises from the present constraint to define STH. For Ka HS, a high sensitivity is achieved at the expense of a degraded vertical resolution from 125 m to 250 m, so that contiguous 6 bins inevitably require that STH should be 1.5 km at minimum. In order to avoid this obvious deficiency, the Ka HS STH is recalculated with a series of thresholds defined under 3 successive bins instead of 6 bins. As a result, shallower STHs less than 1.5 km that are undetected in the 6-bin thresholds can be detected for Ka HS and its histogram seems to more naturally capture low-topped precipitation (Fig. 1d). In the remainder of the paper, STH detection of Ka HS is defined as three successive bins with the 12 dBZ threshold while the reference STH is adopted as it is for Ku and Ka MS.

Figure 2 shows the height-latitude histogram of STH in order to demonstrate the STH statistics in the context of global precipitation climatology. The overall distribution is similar across all the radar products, although Ka MS somewhat underestimates the occurrence frequency of high echo tops compared to Ku and Ka HS as expected from Fig. 1. The higher frequencies around 5 km in Figs. 2b, e is expected by Fig. 1b which has a spike around freezing height. The STH frequency is concentrated below 2 km for latitudes higher than 60° for the both hemispheres, where moderate precipitation from snow and light rain is typical (Behrangi et al. 2014). Over tropical oceans (30°S−30°N, Figs. 2a, b, c), dual peaks corresponding to shallow cumuli at 2 km and deeper clouds at 5 km height are seen while the shallow peak is missing over land. This result is consistent with the TRMM PR study by Short and Nakamura (2000). Subtropical oceans (15°−30°), more notably in the southern hemisphere than in the northern hemisphere, only exhibit a shallow peak as one might expect for regions capped with the trade inversion.

Figure 3 shows the STH histogram for three different meridional zones of the tropics (30°S−30°N), northern extratropics (30°N−65°N), and southern extratropics (65°S−30°S) with oceans and lands separated for each zone. The Ka MS histogram exhibits a notable difference from the other two, where the Ka MS mode tends to miss high echo tops (4−7 km for Figs 3a, d, 7−12 km for Figs. 3b, e, 4.5−7 km for Figs. 3c, f) and is as a result biased toward low echo tops. The Ka MS fails to detect solid precipitation echoes above the freezing height more frequently than Ku and Ka HS, while generally sensitive to the melting layer (Okamoto et al. 2004). As a result, in the tropics (Figs. 3b, e) the Ka MS histogram has a striking spike at 4−5 km, because STH settles down on the melting layer whenever ice particles aloft remain undetected. On the other hand, the Ka HS and Ku histograms stay closely together, implying that the sensitivity advantage of the Ka HS mode may not be as distinct as expected. A closer inspection, however, reveals that the Ka HS better captures shallowest echo tops below 1.5 km than the Ku as highlighted by green and red shades in Fig. 3. Such precipitation with low STHs typically produces light rain with small raindrops and drizzles or light snow with fluffy snowflakes, which are generally difficult to capture at low microwave frequencies. Moreover, one might argue that the Ka HS is also superior in the ability to measure solid precipitation at 11 km or higher in deep convection over tropical continents (Fig. 3e), whereas there is no such evidence outside the tropics. Overall, the histograms suggest faint hints of the Ka superiority to the Ku in terms of sensitivity, although the differences are minor. The Ka HS sensitivity advantage was also pointed out by Kotsuki et al. (2014).

Figure 3 contains both liquid and solid precipitation, but the radar detectability depends on the phase of hydrometeors. To separate rain from snow, Fig. 4 shows the STH histogram with snowfall isolated out, defined where surface air temperature at 2 m is below 0°C. The tropical latitudes never meet this criterion and are not shown. The histograms become somewhat sharpened around low STHs, i.e., snow tend to have lower STHs than rain, but are otherwise similar to the previous figures. It follows that the Ka sensitivity to snow may slightly outperform the Ku although the advantage is small.

5. Discussion and conclusions

This paper is aimed at an early evaluation of the GPM DPR performance with focus on exploring the expected difference in

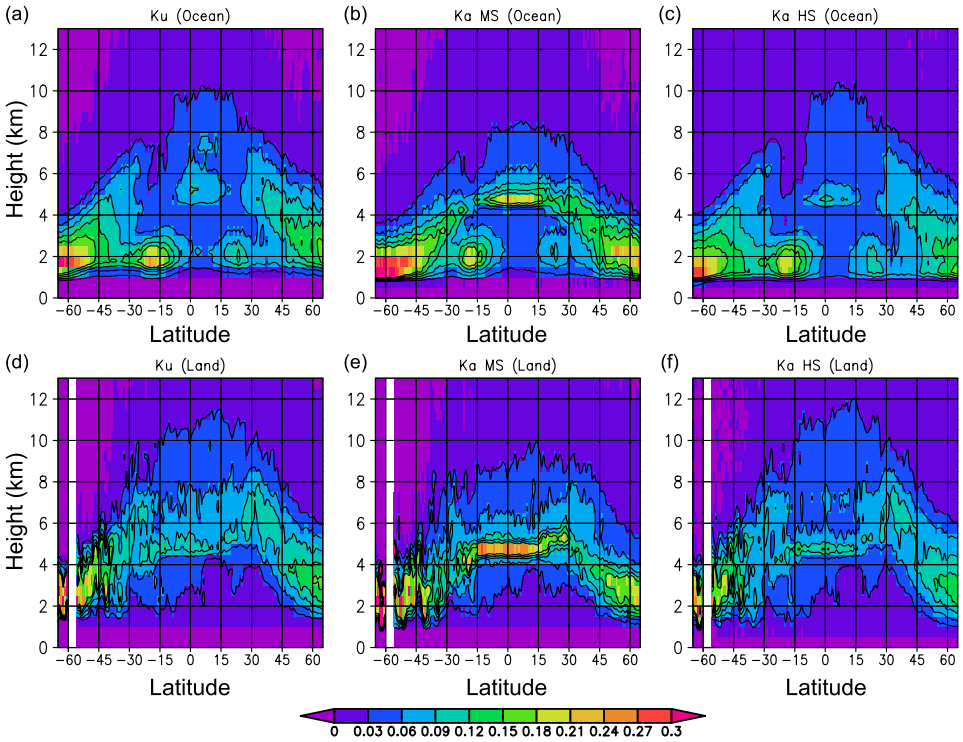

Fig. 2. The height-latitude histogram of STH. The frequency of occurrence is normalized at each latitude. (a) Ku Ocean, (b) Ka MS Ocean, (c) Ka HS Ocean, (d) Ku Land, (e) Ka MS Land, and (f) Ka HS Land. The contour lines are drawn at each 0.03 step up to 0.15.

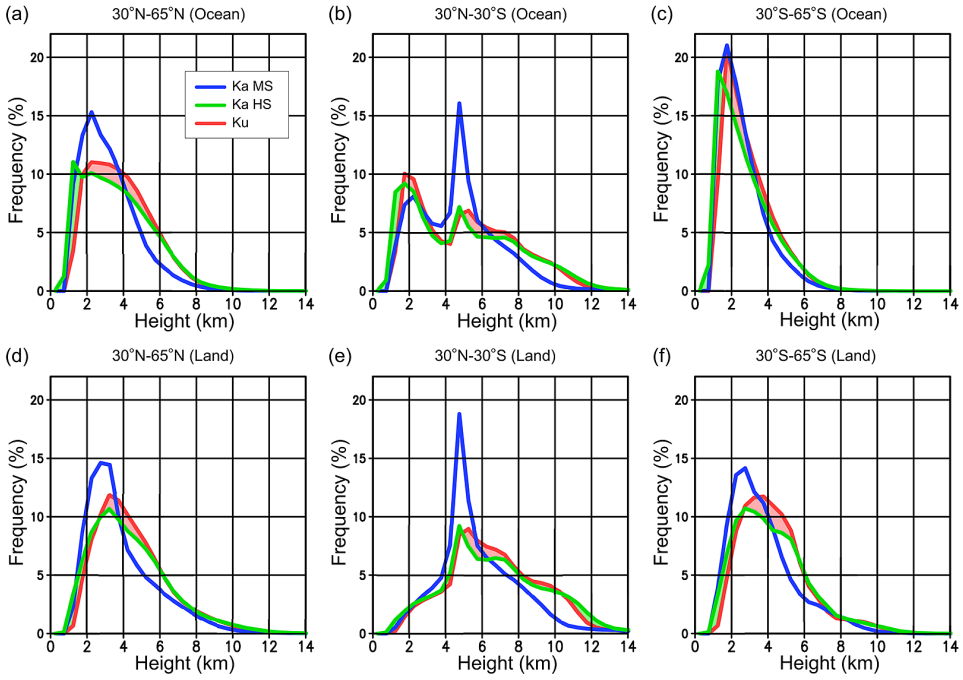

Fig. 3. The STH histogram for Ku, Ka MS, and Ka HS for (a) 30°N−65°N ocean, (b) 30°S−30°N ocean, (c) 30°S−65°S ocean, (d) 30°N−65°N land, (e) 30°S−30°N land, and (f) 30°S−65°S land. For visual clarity, the difference between Ku and Ka HS is shaded in red where Ku exceeds Ka HS and in green otherwise.

precipitation detectability between the Ku- and Ka-band radars. Our interest is to understand to what extent the Ka-band radar is able to detect weak rain and solid state precipitation compared to Ku-band radar. The detectability of the Ku-band radar and two modes of the Ka-band radar (Ka MS and Ka HS) is studied in terms of STH. STH for the Ka HS is redefined with a modified criterion so as to avoid the underrepresentation of shallow precipitation that was found in the original definition. While the Ka MS is found to be least sensitive to high echo tops, the sensitivity advantage of the Ka HS over the Ku is not very evident. A close examination suggests that the Ka HS may be slightly better at capturing weak rain and snow, although the differences are minor.

The difference in sensitivity among different radar frequencies has been studied previously in various contexts. Berg et al. (2009) investigated the precipitation detectability of the TRMM PR and CloudSat W-band radar in attempt to construct the histogram over a full range of precipitation rate beyond the capability of individual instruments. The possibility to separate the liquid and ice phases of precipitation was explored by utilizing the sensitivity difference between the Ku and Ka bands (Liao and Meneghini 2011).

The absence of apparent superiority of the Ka-band radar in terms of precipitation detectability is in part owing to the non-Rayleigh scattering effect. While the Rayleigh approximation marginally holds at the Ku band with the exception of heaviest

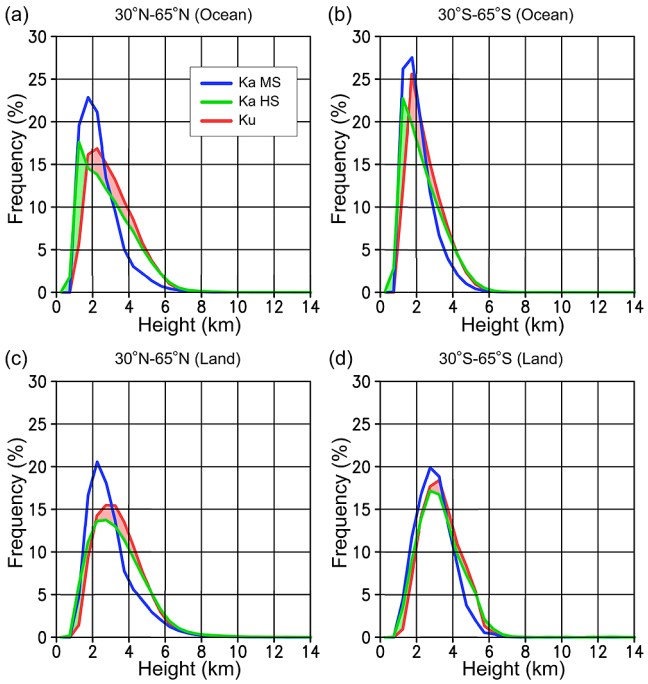

Fig. 4. The same as Figs. 3a, c, d, f, but only for the regions where surface air temperature at 2 m is below 0°C. (a) 30°N−65°N ocean, (b) 30°S−65°S ocean, (c) 30°N−65°N land, and (d) 30°S−65°S land.

rain events, it is no longer valid at the Ka band for a broad range of rain rate (L'Ecuyer and Stephens 2002). This difference in the degree to which the Rayleigh approximation is violated would introduce a frequency dependence in radar reflectivity expressed in dBZ (e.g., Matrosov 1992), generally leading to smaller values at the Ka band than at the Ku. The effect should partly offset the sensitivity advantage of the Ka HS over the Ku, and probably accounts for the current finding that the Ka HS seems not to considerably exceed the Ku in the ability to detect light rain and snow. A quantitative assessment of the non-Rayleigh effect is left for future studies.

Another possible factor to take into account is that the actual Ku-band radar detectability turned out to outperform the original instrumental design and effectively offset the superiority of Ka HS to some extent. The minimum detectable echo of the Ku-band radar was nominally 18 dBZ (Hou et al. 2014), while it was as good as 14.5 dBZ in the pre-launch test. It should be also noted that this current analysis period is limited to 5 months of boreal spring summer. Snow and light rain in the northern hemisphere winter are not included and could potentially affect the representativeness of the present statistics. Future analysis is underway to address these outstanding issues.

Acknowledgements

This analysis is supported by JAXA. GPM DPR standard product was obtained from JAXA. The authors would like to thank Dr. Takuji Kubota (JAXA/EORC) for valuable information of GPM DPR. The JRA55 is jointly developed the Japan Meteorological Agency (JMA) and the Central Research Institute of Electric Power Industry (CRIEPI) and obtained from JMA.

References

Behrangi, A., G. Stephens, R. F. Adler, G. J. Huffman, B. Lambrigtsen, and M. Lebsock, 2014: An update on oceanic precipitation rate and its zonal distribution in light of advanced observations from space. *J Climate*, **27**, 3957−3965.

Berg, W., T. L'Ecuyer, and J. M. Haynes, 2010: The distribution of rainfall over oceans from spaceborne radars. *J. Appl. Meteor. Climatol.*, **49**, 535−543.

Chandrasekar, V., H. Fukatsu, and K. Mubarak, 2003: Global mapping of attenuation at Ku- and Ka-band. *IEEE Trans. Geosci. Remote Sens.*, **41**, 2166−2176.

Hou, A. Y., G. Skofronick-Jackson, C. D. Kummerow, and J. M. Shepherd, 2008: *Global precipitation measurement: Advances in measurement, estimation and prediction*, Springer Berlin Heidelberg, 131−169.

Hou, A. Y., R. K. Kakar, S. Neeck, A. A. Azarbarzin, C. D. Kummerow, M. Kojima, R. Oki, K. Nakamura, and T. Iguchi, 2014: The Global Precipitation Measurement (GPM) mission. *Bull. Amer. Meteor. Soc.*, **95**, 701−722.

Kobayashi, S., Y. Ota, Y. Harada, A. Ebita, M. Moriya, H. Onoda, K. Onogi, H. Kamahori, C. Kobayashi, H. Endo, K. Miyaoka, and K. Takahashi, 2015: The JRA-55 reanalysis: General specifications and basic characteristics. *J. Meteor. Soc. Japan*, **93**, doi:10.2151/jmsj.2015-001.

Kotsuki, S., K. Terasaki, and T. Miyoshi, 2014: GPM/DPR precipitation compared with a 3.5-km-resolution NICAM simulation. *SOLA*, **10**, 204−209.

Kubota, T., N. Yoshida, S. Urita, T. Iguchi, S. Seto, R. Meneghini, J. Awaka, H. Hanado, S. Kida, and R. Oki, 2014: Evaluation of precipitation estimates by at-launch codes of GPM/DPR algorithms using synthetic data from TRMM/PR observations. *IEEE J-STARS.*, 1−15.

Kumagai, H., T. Kozu, and T. Igucshi, 1997: Rain/no-rain discrimination for TRMM precipitation radar. *IEEE Trans. Geosci. Remote Sens.*, **3**, 1111−1113.

L'Ecuyer, T. S., and G. L. Stephens, 2002: An estimation-based precipitation retrieval algorithm for attenuating radars. *J. Appl. Meteor.*, **41**, 272−285.

Liao, L., and R. Meneghini, 2005: A study of air/space-borne dual-wavelength radar for estimation of rain profiles. *Adv. Atmos. Sci.*, **22**, 841−851.

Liao, L., and R. Meneghini, 2011: A study on the feasibility of dual-wavelength radar for identification of hydrometeor phases. *J. Appl. Meteor. Climatol.*, **50**, 449−456.

Liao, L., R. Meneghini, T. Iguchi, and A. Detwiler, 2005: Use of dual-wavelength radar for snow parameter estimates. *J. Atmos. Oceanic Technol.*, **22**, 1494−1506.

Matrosov, S. Y., 1992: Radar reflectivity in snowfall. *IEEE Trans. Geosci. Remote Sens.*, **30**, 454−461.

Okamoto, K., H. Sasaki, E. Deguchi, and M. Thurai, 2004: Bright-band height statistics observed by the TRMM precipitation radar. *The 2nd TRMM International Science Conference*.

Rose, C. R., and V. Chandrasekar, 2005: A systems approach to GPM dual-frequency retrieval. *IEEE Trans. Geosci. Remote Sens.*, **43**, 1816−1826.

Seto, S., T. Iguchi, and T. Oki, 2013: The basic performance of a precipitation retrieval algorithm for the global precipitation measurement mission's single/dual-frequency radar measurements. *IEEE Trans.Geosci. Remote Sens.*, **51**, 5239−5251.

Short, D. A., and K. Nakamura, 2000: TRMM radar observations of shallow precipitation over the tropical oceans. *J. Climate*, **13**, 4107−4124.

Takahashi, N., and T. Iguchi, 2008: Characteristics of TRMM/PR system noise and their application to the rain detection algorithm. *IEEE Trans. Geosci. Remote Sens.*, **46**, 1697−1704.

Manuscript received 30 October 2014, accepted 27 December 2014
SOLA: https://www.jstage.jst.go.jp/browse/sola/